Open Research Online

Responsivity mapping techniques for the non-positional CCD: the swept charge device CCD236

Conference or Workshop Item

How to cite:

Smith, P.; Murray, N.; MacCormick, C.; Gow, J.; Weatherill, D.; Allanwood, E.; Pool, P. and Holland, A. (2013). Responsivity mapping techniques for the non-positional CCD: the swept charge device CCD236. In: UV, X-Ray, and Gamma-Ray Space Instrumentation for Astronomy XVIII, SPIE, article no. 8859-21.

For guidance on citations see FAQs.

Version: Accepted Manuscript

Link(s) to article on publisher's website:
http://dx.doi.org/doi:10.1117/12.2028865

oro.open.ac.uk

Responsivity mapping techniques for the non-positional CCD; the swept charge device CCD236

P. H. Smith*[a], N. J. Murray[a], C.MacCormick[a], J. P. D. Gow[a], D. Weatherill[a], E. Allanwood[a], P. Pool[b], A. D. Holland[a],

[a]e2v centre for electronic imaging, Open University, Walton Hall, Milton Keynes, MK7 6AA, UK,
[b]e2v technologies plc, 106 Waterhouse Lane, Chelmsford, CM1 2QU, UK,
*p.h.smith@open.ac.uk

ABSTRACT

The e2v CCD236 is a swept charge device (SCD) designed as a soft X-ray detector for spectroscopy in the range 0.8 keV to 10 keV [1]. It benefits from improvements in design over the previous generation of SCD (the e2v CCD54) [2] to allow for increased detector area, a reduction in split X-ray events and improvements to radiation hardness [3]. To enable the suppression of surface dark current the device is clocked continuously, therefore there is no positional information making responsivity variations difficult to measure. This paper describes investigated techniques to achieve a responsivity map across the device using masking and XRF, and spot illumination from an organic light-emitting diode (OLED). The results of this technique should allow a deeper understanding of the device sensitivity and allow better data interpretation in SCD applications.

Keywords: Swept Charge Device (SCD), CCD236, soft X-ray detector, X-ray fluorescence (XRF), responsivity mapping, OLED.

1.   INTRODUCTION

The e2v technologies plc. CCD236 swept charge device (SCD) is one of the second generation of SCD developed for X-ray spectroscopy [1]. With over 4 cm^2 of detection area this new SCD represents one of the largest area, high operating temperature XRF detectors available. The first generation of the SCD, the CCD54 was used in the European Space Agency's Demonstration of a Compact X-ray Imaging Spectrometer (DCIX) instrument [4] in 2003 and India's Chandrayaan-1 X-ray Spectrometer (C1XS) instrument in 2008 [5]. The second generation of device, the CCD236 will be used in India's Chandrayaan-2 Large Soft X-ray Spectrometer (CLASS) instrument [6] and China's Hard X-ray Modulation Telescope (HXMT) [7].

To enable the suppression of surface dark current in the device, the device is clocked continually, therefore no positional information is given with the signal. The direction of charge flow across the device can be seen in Figure 1. In conventional charge coupled devices (CCD) responsivity mapping is straightforward - a known flat-field signal is used to illuminate the CCD, which is then read-out to give a level of response per pixel. Since the SCD gives no positional information, alternative methods for achieving a map of responsivity were investigated.

The tests performed included shielding different regions on the device with a copper mask to illuminate specific areas with fluoresced manganese sample in order to measure the performance of different regions of a non-positional device. An organic light emitting diode (OLED) was used to illuminate small regions of the SCD to attain relative measurements at different locations on the device. Finally a synchrotron was used to trace a 3 mm diameter X-ray beam across the device horizontally and vertically to plot a profile of device performance. We describe the method and results, along with a summary of the findings. The device reported here did not undergo any proton irradiations and represents the performance at the start of a space mission using this technology. Measurements were taken at -30 °C.
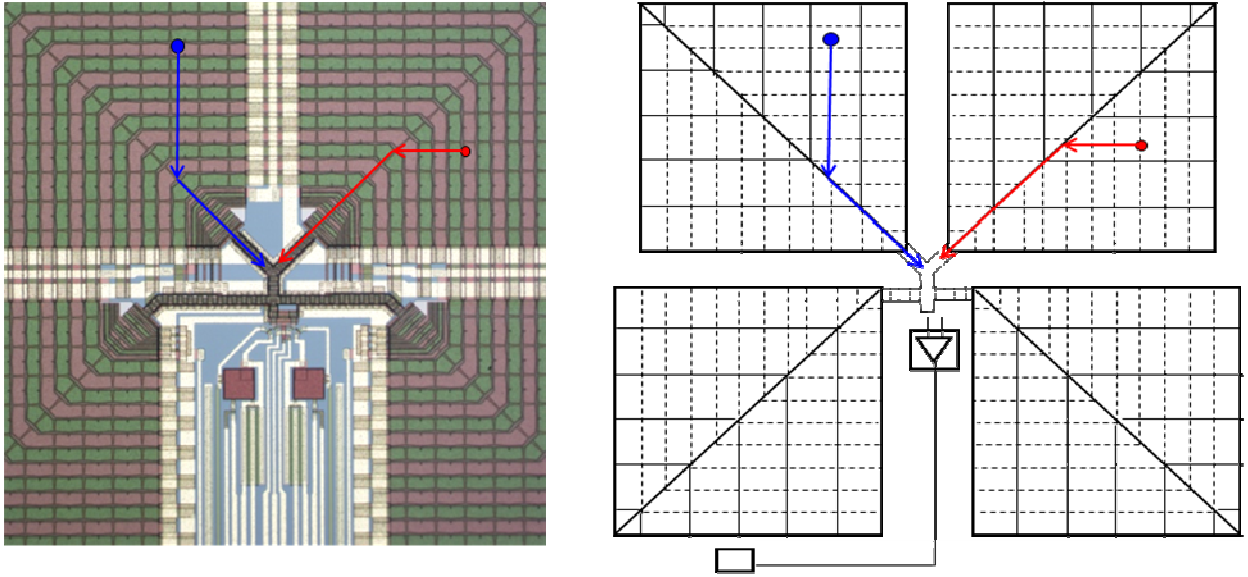
Figure 1: Microscope image (left) and schematic (right) of the central region of CCD236. The red and blue arrows show the direction of charge as it is clocked through the device and read out.

2. EXPERIMENTAL METHODS

In each experiment the CCD236 under test was housed inside the vacuum chamber, illustrated in Figure 2. The CCD236 was mounted onto an aluminium cold finger attached to a three stage thermo electric cooler (TEC) with a 1,000 Ω platinum resistance thermometer fitted to the base of the cold finger. Temperature control to ± 0.1 °C was provided using an ILX Lightwave controller. Due to the temperature gradient between the cold finger and the CCD236 silicon, typically ~0.5 °C, the error on the temperature measurement was taken to be ± 1 °C. A period of 30 minutes was allowed for the device temperature to stabilise. Clock and bias signals were provided using XCAM ltd. CCD drive electronics and software, operating the device at 110 kHz, and the data were recorded onto a laptop computer. This set-up was adapted slightly for each experimental method, as described in the following sections.
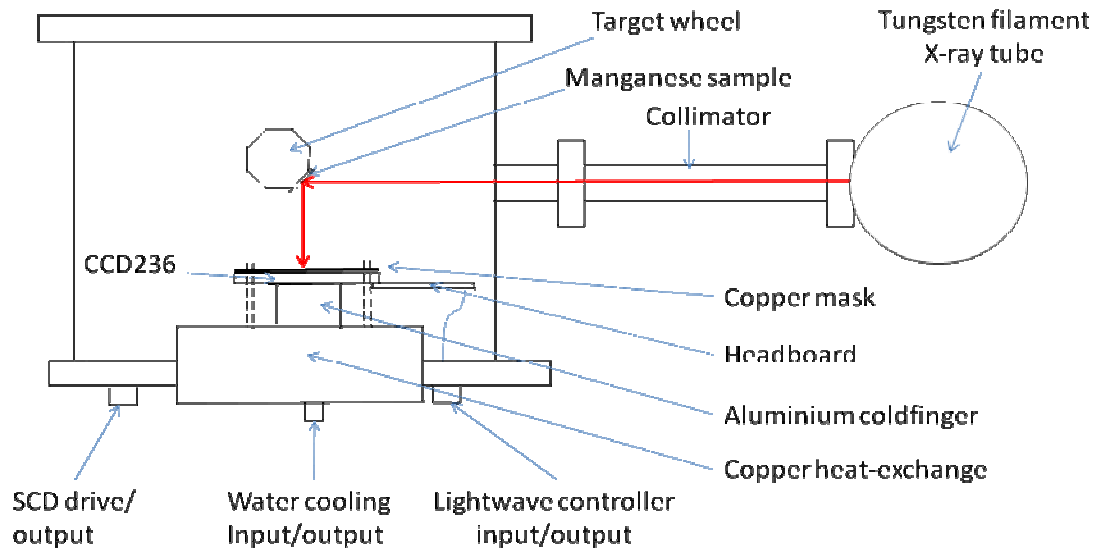
Figure 2: Schematic of SCD camera head using X-ray tube to fluoresce a manganese sample

2.1 Masking

An Oxford Instruments tungsten filament X-ray tube was used to fluoresce a manganese target held on a target wheel at a 45 degree incident angle. The manganese target was used to illuminate the CCD236 with Mn-Kα X-rays. This arrangement enabled a high, steady flux to be applied. Images of 1000 by 1000 samples (as the sensor does not have conventional "pixels") were taken using sufficient clocking to represent such an area. These images were collected using a variety of different copper masks to shield different regions of the detector from incident X-rays. The copper masks were placed over the device on top of a piece of Tufnol (10G) to protect the devices bond wires and ensure there was no shorting. A number of different mask designs were created to shield different regions of the detector, the masks are illustrated in Figures 3 and described below:

a) Original square mask To cover the bond wires and edge of the device. This mask was used to compare other masking areas by normalising against these values. To begin with this mask was rotated to ensure any errors in the symmetry were not effecting the number of events identified. It was found to give the same results with any orientation.

b) Read out amplifier mask Covering only the central read out amplifier.

c) Exposing only the read out amplifier Used to investigate the X-ray interaction in this region

d) Small triangles Covering half of the region in each quadrant. This mask was rotated to give an indication into the performance in each quadrant.

e) Pin-point illumination An array of 1mm diameter holes along the vertical, horizontal and diagonal of one quadrant of the device.

f) Copper foil was used to select each hole in turn for illumination.

The masks were clamped down on nylon threads to eliminate any chance of grounding through contact with the metal PCB mounting. To ensure good statistics for the data produced using each mask the number of times the device was readout was varied, ensuring at least 100,000 counts for each data point. Only isolated X-ray events were used which

were identified using a threshold of three times the standard deviation of the noise peak and plotted as a histogram of energy using MATLAB.

The uniformity of the X-ray beam will be measured using an e2v CCD30-11 to see whether there is any variation in the X-ray profile across the device, and if any count rate fluctuations are an artefact of X-ray beam non-uniformity.
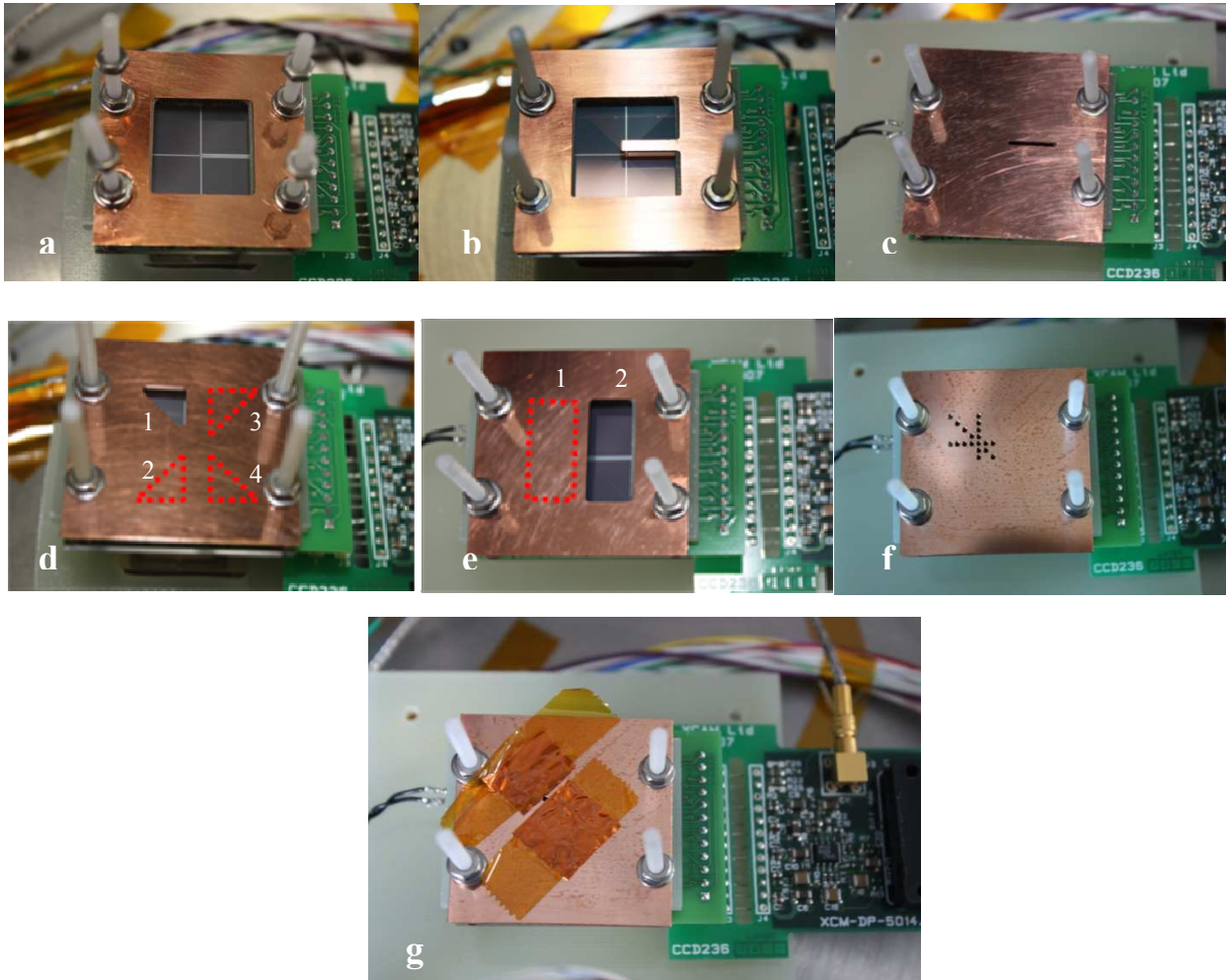

Figure 3: Images of copper masks used during the study to measure the relative count rate in different regions of the device. Details can be read in section 2.1 letters and numbers correspond with the table below.

The results of each area were compared against each other, to obtain a relative count rate across the SCD and results of areas **a** to **e** are summarised in Table 1. As expected the area where only the read-out register was exposed to X-rays had a much lower count rate of around $1/10^{th}$ that of the other imaging areas due to this not being the main sensing part of the detector.

Position	Area (mm^2)	Frames	Effective area (mm^2)	FWHM	Noise (e- r.m.s)	Events
a	400	6	2400	139.8	6.1	121000
b	390	6	2340	139.3	6.6	120000
c	10	240	2400	139.0	6.0	10600
d1	50	48	2400	140.2	6.0	140000
d2	50	48	2400	139.5	6.1	146000
d3	50	48	2400	138.7	6.1	143000
d4	50	48	2400	139.4	6.1	138000
e1	200	12	2400	138.4	6.3	119000
e2	200	12	2400	138.4	6.3	114000

Table 1: Data plot of count rates at different regions on the SCD with frames and exposed area collectively making a comparable effective charge collection area

The positions used during the pinpoint illumination can be seen in Figure 4, where the copper mask array has been overlaid onto an image of a CCD236 to show the approximate positioning of the holes over the device. The data from lines **a**, **b** and **c** are plotted in Figure 5. Position 1 corresponds to the holes nearest the labelling letter and 7 is at the edge of the device. Both the resolution and noise measurements at all locations where found to be around 138 FHWM and 6 e-r.m.s respectively.
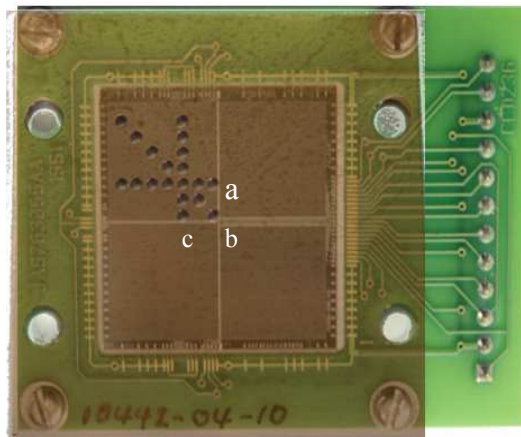

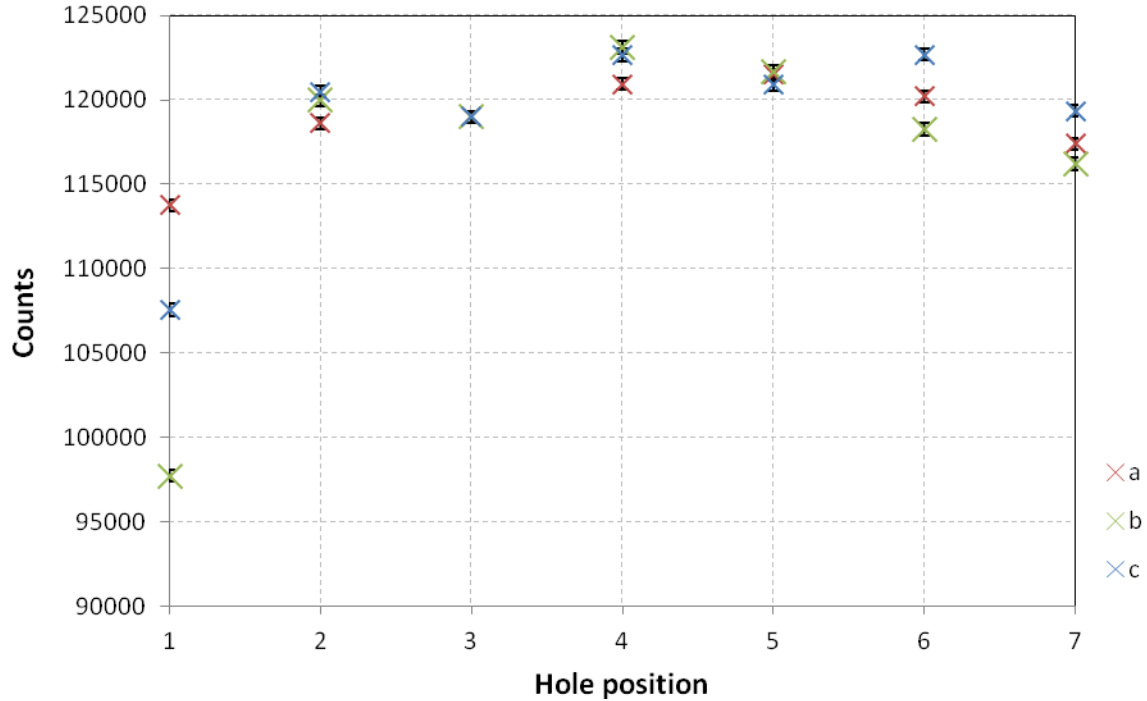Figure 4: SCD image superimposed with pinpoint masking array to show regions investigated

Figure 5: Data plot of count rates at locations shown in Figure 4 across one quadrant of the SCD

The overall the trend line for **a b** and **c** shows a lower count at the start and end (positions 1 and 7) as these were towards the edge of the imaging quadrant so some charge could have been lost to the inactive regions of the device, particularly at position 1 in each case. It is also possible that the X-ray beam is over a non imaging part of the device where the four quadrants meet. Positions 2 to 6 show consistent results.

This method could be extended to the other quadrants of the device, however it is very time consuming with each point taking around seven hours due to the large number of frames required in addition to cooling and vacuum cycling times. X-ray beam uniformity will be measured using an e2v CCD30-11 imaging device in future work.

2.2 O-LED illumination

As a proof of concept for a quicker method of illuminating small regions of the detector at a known location, the use of an organic light emitting diode (OLED) array was investigated. The OLED has a slightly larger area than the SCD and was placed in proximity with the non-imaging SCD to provide a position-dependent signal that could be generated by turning on specific pixels in the array. This has the advantage of saving both time and resources. A BL128128 C2 OLED display was used, with an array of 128 by 128 red green and blue pixels. Each can be turned on and off individually using a bread-boarded drive system, programmed with an ARM cortex-M3 MBED microcontroller. The green portion of each OLED pixel was used to illuminate the SCD as this provided a lower signal level. A 10dB attenuator was used in line with the output signal to avoid saturation. The OLED was mounted above the CCD236 as shown in Figure 6.

In the initial design the OLED was placed close to the SCD without an imaging system to project the light onto specific regions. The light from a single OLED pixel is concentrated in a region of the SCD below, however there is still some illumination over the remaining sensing area of the detector. Ideally, we would like to image the OLED onto a SCD with unit magnification such that the total light emitted from each OLED pixel is collected on the corresponding SCD "sample". This is an area to be investigated in the future.
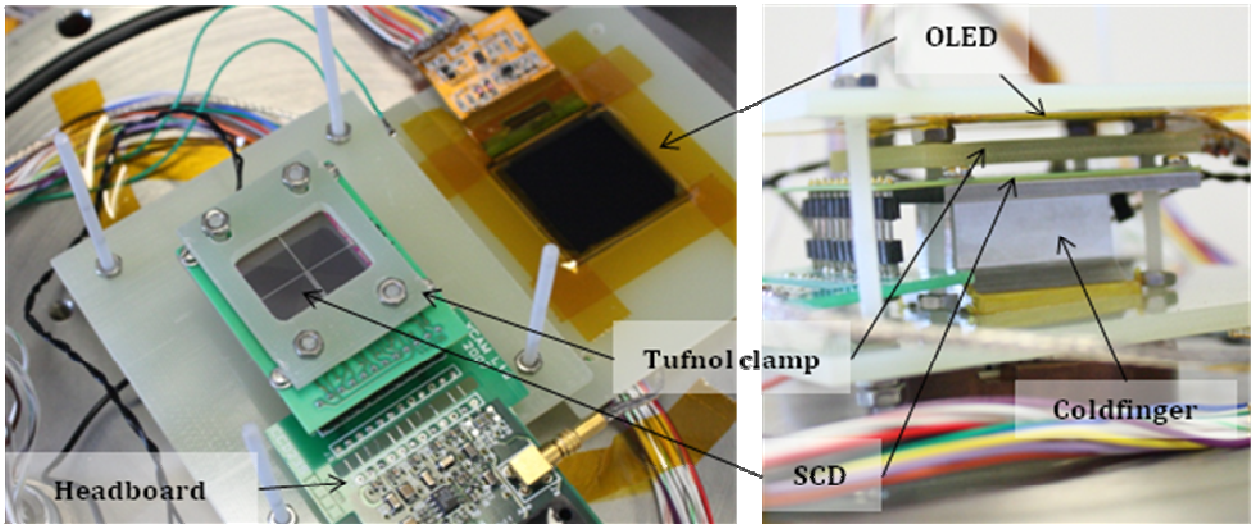
Figure 6: left OLED set-up with SCD and right mounted in position

During testing with the OLED the device was read out continuously. A raster of OLED pixels was then performed with each pixel used for illumination pulsed at a rate of 1 kHz, resulting in the response pulses illustrated in Figure 7 which shows the result from two different OLED pixels. The location of the pulse in relation to the x-axis bears no relation to the location of the OLED pixel, solely depending on when the OLED pixel was pulsed in relation to the number of clock cycles performed thus far for that readout. The area under the pulse was integrated to find the relative photon counts, i.e. signal, for that location. This was then plotted as a 3D graph shown in Figure 8, where the x and y position of each OLED location is plotted against the corresponding signal level at that location. The imaging area is composed of "L" shaped electrodes which vary in length across the quadrant of the device [1]. Charge is summed across these electrodes which results in the ramp profile as seen in Figure 7. The fact that the ramp profile is not a perfect triangle indicates that the incident light is concentrated in a certain region.
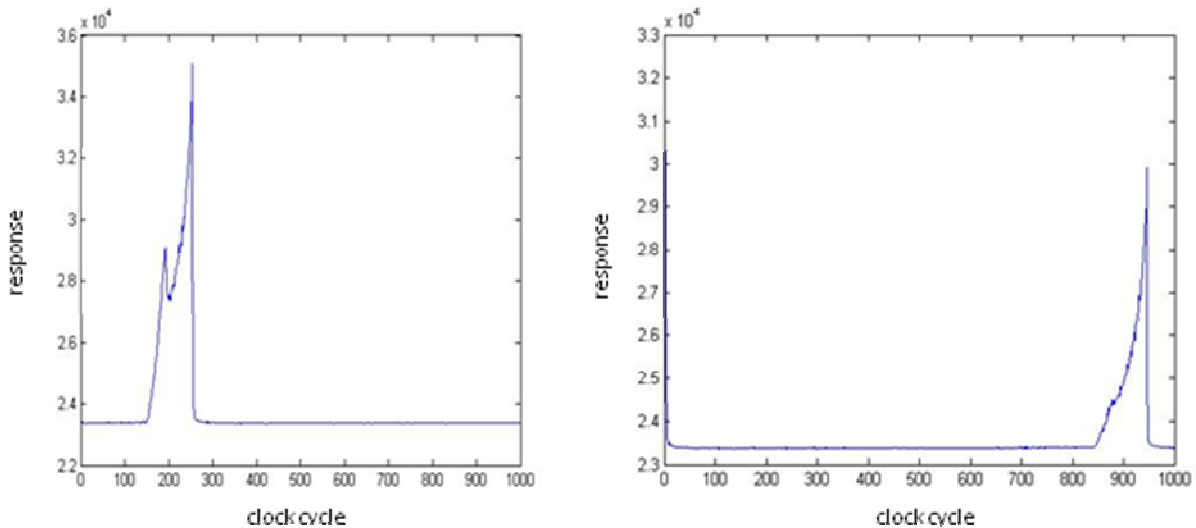

Figure 7: Two examples of relative signal levels at different read-out positions.
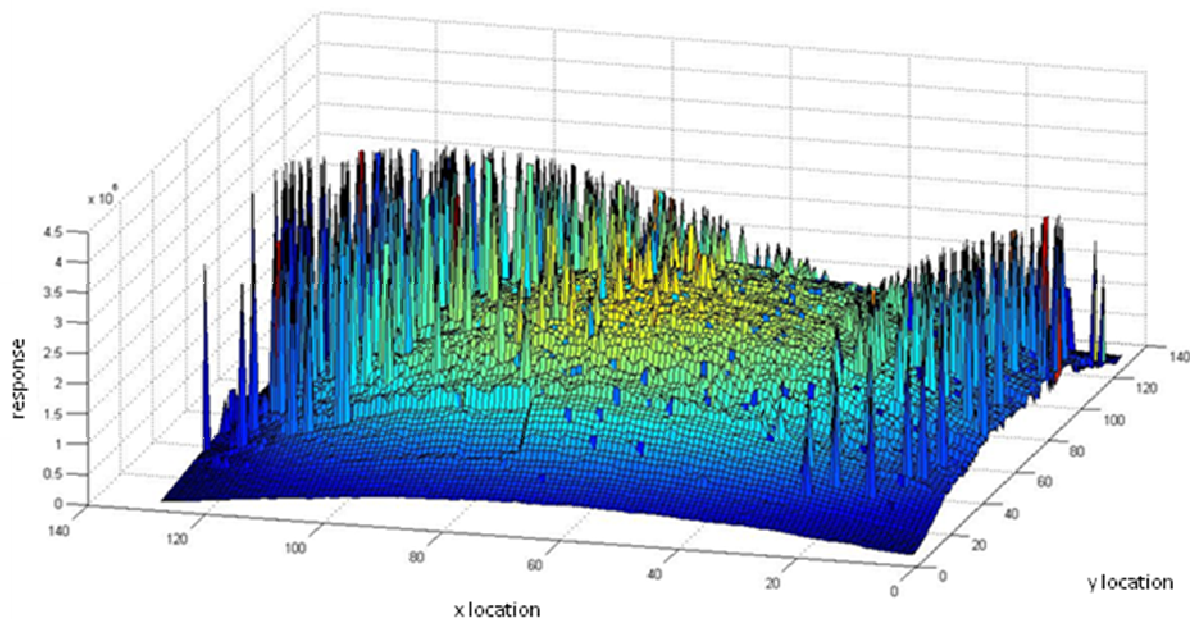
Figure 8: 3D map of relative response across the swept charge device, where the x and y locations represent the OLED location.

The overall underlying structure of the responsivity map shows a paraboloid shape, where the charge in the middle of the device is being summed together with those adjacent, as a larger region of the device was illuminated than that intended. The shape rolls off towards the edges where the illuminated signal is on the edge of the device. The spikey areas are likely to be the result of saturation in the device, or potentially where a slight malfunction with the OLED syncing has caused one of the brighter coloured pixels (red or blue) to turn on instead of the green as intended. This will be investigated in the future. With the inclusion of a lensing system, the uncertainty in the illuminated area would be reduced, thus improving the value of these results.

The uniformity of the OLED light levels will be measured over various pixels sampled throughout the array by imaging its output onto a positional CCD of known regional performance, the e2v CCD 42-10, and rotating by 90 degrees to attain an average and measure any variation seen in these four positions. This will give a map of the OLED light levels which can be used in conjunction with the SCD responsivity map to eliminate the variations in OLED light output.

2.3   Synchrotron pencil beam scan

An X-ray beamline was used at the Physikalisch-Technische Bundesanstalt (PTB) beamline at the Berliner Elektronenspeicherring-Gesellschaft für Synchrotronstrahlung (BESSY II) facility. The facility was used to create a pencil beam which was moved over the SCD to accurately map spectral response with position. The chamber was connected to the beamline through a 2¾ inch (DN35CF) metal adaptor port at the back of the vacuum chamber. During that time, a horizontal and vertical scan of a 10 keV beam of photons with a 3 mm spot size was conducted.

To ensure the beam was hitting the sensitive area of the detector, the beam was aligned by taking readings with the beam at different positions in first the x and then the y axis and recording the number of X-rays detected. The beam was moved in 1mm increments until no X-rays were detected or the limit of the translation stage in the beamline was reached. It was assumed that the point where the count rate dropped was the edge of the SCD.

A profile of X-ray counts in the x and y axis is illustrated in Figure 9, an image of a CCD236 showing relative positions for reference can be seen in Figure 10. The maximum plateau area in each dimension maps the central region of the imaging quarter. The reduction in counts across the y-axis marks the read-out area of the device, and the reduction in counts across the x-axis marks the transition from one imaging quadrant to the other.
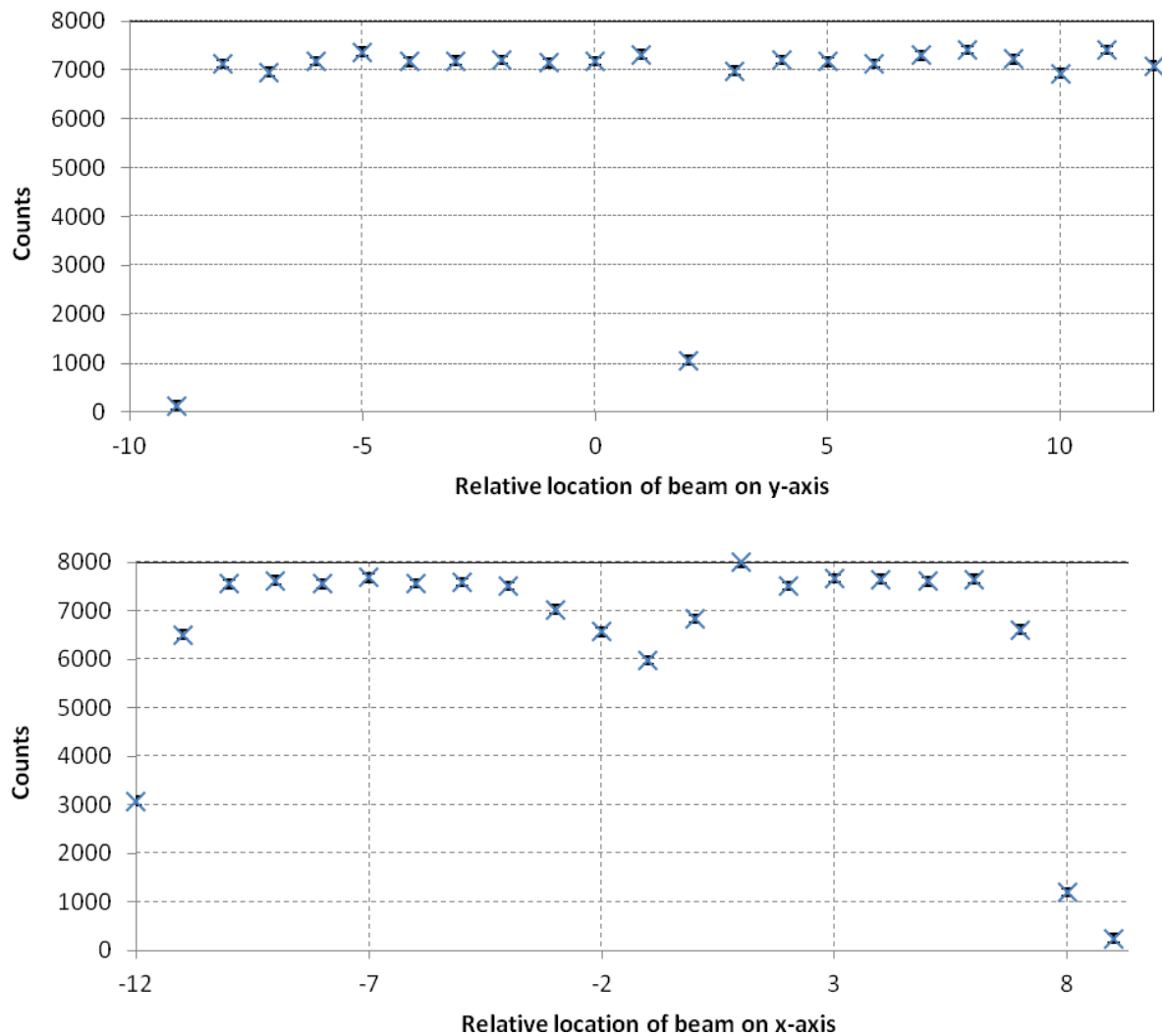

Figure 9: A profile of X-ray counts in the y direction (top) and x direction (bottom) while scanning a 3mm by 3mm X-ray beam across the device.
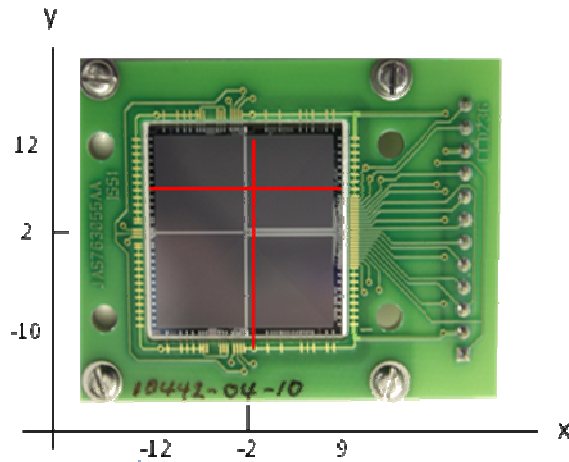
Figure 10: Image of CCD236 overlaid with beam trace at the relative x and y position on each axis

3. DISCUSSIONS AND FUTURE WORK

The three different experimental methods have shown that it is possible to map the responsivity of a non-positional device to various precision and accuracies. The masking technique is very time consuming, where multiple frames are required for the count rate to be significant. The thermal and vacuum cycling between points is also undesirable. It does however give a truer representation of the low flux X-ray environment in which the SCD devices will be use. Measuring the X-ray beam uniformity of the experimental set-up will improve the confidence in these results.

The OLED method shows promising results. A map of the entire device was produced in a relatively short amount of time taking hours rather than days which were required for the masking technique. The device could remain cool and under vacuum for the duration of the tests, as the OLED pixels were turned on and off through computer control. The diffusion of the light due to the lack of a lensing system meant that signal combination occurred, resulting in a higher charge count in the centre of the device. However, a simple solution is to use an optical system to project each OLED pixel into a single SCD pixel, improving the accuracy and precision of this method. Measuring the OLED signal variation with position will allow a better 3D responsivity map to be produced, where spatial variation of the OLED signal can be subtracted from the results, to better characterise the SCD. The output intensity as a function of position will need to be determined, e.g. through using a conventional imaging CCD system before being used on the non-imaging SCD.

For precision, the use of an X-ray beamline at a synchrotron facility is preferable. The X-ray beamline can be selected to the required energy, and assuming the device is mounted level and flat to the beamline, the position on the device can be deduced. Despite the advantages, the cost of this method is prohibitive to testing a large number of devices and is limited to specific facilities. Also, future measurements would ideally be made using a smaller beam diameter (e.g. 100 microns). However, the existing data shows the drop in efficiency across the centre of the device where the device is not sensitive to signal.

4. CONCLUSIONS

The masking and pencil beam scan methods both show comparable results with a uniform performance across the main sensing regions of the SCD, they also show a reduction in signal across the inactive regions of the device. Both techniques agree well and conclude that there is no count rate change with position. The OLED technique will need a lensing system and a method of removing any variation with illumination across its pixels before it can be used to produce comparable results, however, with improvements this novel technique shows promise as an alternative method.

The responsivity mapping of a non-positional detector is useful particularly for space XRF applications, where the abundance information is important. This will also important in comparing pre and post irradiated devices to gain a better understand of charge transfer efficiency through the device. Minimising the errors from the detector would mean the main contribution of errors come from factors outside the detector system, improving confidence in the results.

5. REFERENCES

[1] Holland, A. D., and Pool, P. J., "A New Family of Swept Charge Devices (SCDs) for X-ray Spectroscopy Applications", High Energy, Optical and Infrared Detectors for Astronomy III Proc. SPIE, (2008).

[2] Lowe, B. G., Holland, A. D., Hutchinson, I. B., Burt, D. J., and Pool, P. J. "The Swept Charge Device, a novel CCD-based EDX Detector: First Results", Nuclear Instruments and Methods in Physics Research A **458** pp. 568-579, (2001).

[3] Gow, J., Holland, and A. D., Pool, P., "Proton Radiation Damage Study of the Next Generation of Swept Charge Devices", UV, X-Ray and Gamma-Ray Space Instrumentation for Astronomy XVI Proc. SPIE, (2009).

[4] Grande, M., "The D-CIXS X-ray spectrometer on ESA's SMART-1 Mission to the Moon", Earth, Moon and Planets, **85-86** pp. 143-152, (2001).

[5] Grande, M., Maddison, B. J., Howe, C. J., Kellett, B. J., Sreekumar, P., Huovelin, J., Crawford, I. A., Duston, C. L., Smith, D., Anand, M., Bhandari, N., Cook, A., Fernandes, V., Foing, B., Gasnaut, O., Goswami, J.N., Holland, A., Joy, K. H., Kochney, D., Lawrence, D., Maurice, S., Okada, T., Narendranath, S., Pieters, C., Rothery, D., Russell S.S., Shrivastava, A., Swinyard, B., Wilding, M., and Wieczorek, M., "The C1XS X-ray Spectrometer on Chandrayaan-1", Elsevier, Planetary and Space Science **57** pp.717-724, (2009).

[6] Radhakrishna, V., Narendranath, S., Tyagi, A., Bug, M., Unnikrishnan, U., Kulkarni, R., Sreekantha, C.V., Kumar, Balaji, G., Athiray, P.S., Sudhakar, M., Manoj, R., Chetty, S. V., Thyagaraj, M. R., Howe, C., Gow, J., and Sreekumar P. "The Chandrayaan-2 Large Area Soft X-ray Spectrometer (CLASS)", 42nd Lunar and Planetary Science Conference, 1708, (2011).

[7] Wu, Y. P., Ren, D. H., and You, Z., "HXMT Satellite for Space Hard X-ray Observation", Advances in Space Research **34** pp. 2667-2672 (2004).